Available online at www.sciencedirect.com
SCIENCE DIRECT
Trans. Nonferrous Met. Soc. China 17(2007) 389−393
Transactions of Nonferrous Metals Society of China
www.csu.edu.cn/ysxb/

Nanostructured yttria stabilized zirconia coatings deposited by air plasma spraying

ZHOU Hong(周 洪), LI Fei(李 飞),
HE Bo(何 博), WANG Jun(王 俊), SUN Bao-de(孙宝德)

State Key Laboratory of Metal Matrix Composites, Shanghai Jiao Tong University, Shanghai 200030, China

Received 13 September 2006; accepted 4 January 2007

Abstract: Nanostructured yttria partially stabilized zirconia coatings were deposited by air plasma spraying with reconstituted nanosized powder. The microstructures and phase compositions of the powder and the as-sprayed nanostructured coatings were characterized by transmission electron microscopy(TEM), scanning electron microscopy(SEM) and X-ray diffraction(XRD). The results demonstrate that the microstructure of as-sprayed nanostructured zirconia coating exhibits a unique tri-modal distribution including the initial nanostructure of the powder, equiaxed grains and columnar grains. Air plasma sprayed nanostructured zirconia coatings consist of only the nontransformable tetragonal phase, though the reconstituted nanostructured powder shows the presence of the monoclinic, the tetragonal and the cubic phases. The mean grain size of the coating is about 42 nm.

Key words: yttria; zirconia; plasma spraying; thermal barrier coatings; nanostructure

1 Introduction

Nanostructured materials are characterized with grain size less than 100 nm in at least one dimension. When the grain size becomes smaller, more atoms are associated with grain boundaries or interfacial boundaries compared with crystal lattice sites. Thus, the properties of nanostructured material are altered by the grain size effect due to the large volume fraction of internal interface[1−2]. Nanostructured materials, which are in their infancy of development, have demonstrated many superior properties over conventional coarse-grained counterparts including the enhanced solubility, good corrosion resistance, lower sintering temperature, improved ductility, hardness, toughness and strength, etc.[1−5].

Thermal barrier coatings(TBCs) have been extensively applied to hot section components in the aerospace industry as an insulation system. Conventional TBCs usually consist of 6%−8% (mass fraction) yttria partially stabilized zirconia(YPSZ) top coat with about 100−500 μm in thickness for the low thermal conductivity combined with proper chemical stability at high temperatures, and a MCrAlY (M=Ni and/or Co) oxidation-resistant metallic bond coat. The use of the conventional ceramic coatings deposited by either air plasma spraying(APS) or electron beam physical vapor deposition(EB-PVD), together with internal cooling of underlying superalloy components, could sustain a reduction of up to 300 ℃ on the surface of the superalloy, hence improving the efficiency and performance of engine[6−8]. Recently, the nanostructured coatings by thermal spraying have received widely interest because of their extraordinary properties. It was reported that nanostructured YPSZ coatings had good wear and erosion resistance, low thermal conductivity, high coefficient of thermal expansion, excellent thermodynamic and mechanical properties toward thermal cycling in the gas turbine environment[9−15]. Therefore, nanostructured TBCs are expected to provide better performance than the conventional ceramic coatings.

In the current work, zirconia-based nanostructured TBCs were fabricated by air plasma spraying with reconstituted nanostructured powder. The aim of this work is to investigate the microstructure and phase composition of the nanostructured ceramic coatings.

Foundation item: Project supported by the Scientific Research Fund of Youth Teacher in Shanghai Jiaotong University
Corresponding author: SUN Bao-de; Tel: +86-21-62932914; E-mail: bdsun@sjtu.edu.cn

2 Experimental

2.1 Sample preparation and coating

Disks of annealed state titanium alloy (Ti-6.6Al-3.61Mo-1.69Zr-0.28Si, mass fraction, %) with 80 mm in diameter and 3 mm in thickness were used as substrates. After finally polished to 38 μm abrasive, the substrates were grit blasted with alumina, ultrasonically cleaned in anhydrous ethylene alcohol and dried in cold air prior to coat deposition. Commercial available reconstituted nanosized 8% YPSZ powder (DDN, Cug-nano, Hubei, China) with a particle size range of 20−70 μm and Ni-20Cr-6Al-Y metal powder (HHNiCrAlY-9, CAAMS, Beijing, China) with particle size ranging from 10 to 100 μm were used.

The NiCrAlY bond coat of about 100 μm in thickness was deposited by air plasma spraying onto the titanium alloy substrate before the YPSZ coat of about 300 μm in thickness was sprayed using an air plasma spray system (DH80, CAAMS, Beijing, China). No air cooling on the back side of the substrates was applied during the spraying process. In order to retain the preexisting nanostructure of the feedstock, it is necessary to partially melt the powder particles. The spraying parameters are listed in Table 1.

Table 1 Spraying parameters for nanostructured TBCs

TBC	Current/A	Voltage/V	Primary gas flow rate/(L· min^{-1})	
			Ar	N_2
NiCrAlY	480	65	36.7	−
YPSZ	500	70	−	36.7

TBC	Secondary gas flow rate (H_2)/(L ·min^{-1})	Carrier gas flow rate (Ar)/(L ·min^{-1})	Powder feeding rate/ (g·min^{-1})	Spray distance/ mm
NiCrAlY	3−5	3.5	54.4	100
YPSZ	3−5	3.0	10.4	70

2.2 Characterization of powder and as-sprayed coatings

The nanosized particles were observed with a transmission electron microscopy (TEM, Model JEM-2010, Tokyo, Japan). The morphologies of the reconstituted powder and the nanostructured coatings were characterized by a field emission scanning electron microscope (FESEM, Model FEI Sirion 200, USA). The phase compositions of feedstock and coating were examined by a X-ray diffractometer (XRD, Model D8, Bruker, Germany) operated with Cu K_α radiation (λ= 0.154 056 nm). XRD was also used to estimate the average grain size of the as-sprayed coatings by using the Scherrer equation:

$$B(2\theta)=0.9\lambda/D\cos\theta \quad (1)$$

where $B(2\theta)$ is the true broadening of the diffraction line measured at half-maximum intensity, which is also known as full-width at half-maximum (FWHM); D is the mean dimension of grain; λ is the wavelength of the X-ray radiation and θ is the Bragg angle. The correction for instrumental broadening was taken into consideration in the measurement of the peak broadening by comparing the widths at half maximum intensity of X-ray reflection between the sample and the single crystalline Si standard, and then Cauchy correction was used to remove the instrumental broadening to obtain the true crystal broadening.

$$B_p^2(2\theta)=B_h^2(2\theta)-B_f^2(2\theta) \quad (2)$$

where $B_p(2\theta)$ is the true half maximum width; $B_h(2\theta)$ and $B_f(2\theta)$ are the half maximum widths of the sample and the single crystalline Si standard, respectively. The applicability of this method was confirmed by comparing results from TEM and XRD according to Refs.[16−17].

3 Results and discussion

3.1 Morphology observation

Fig.1 shows the TEM micrograph of the nanosized YPSZ particles and the SEM micrograph of the agglomerated YPSZ powder. It can be seen that the size of nanoparticles ranges from 20 to 30 nm. The nanoparticles have to be reconstituted into micron-sized spherical granules by spray-drying process before plasma

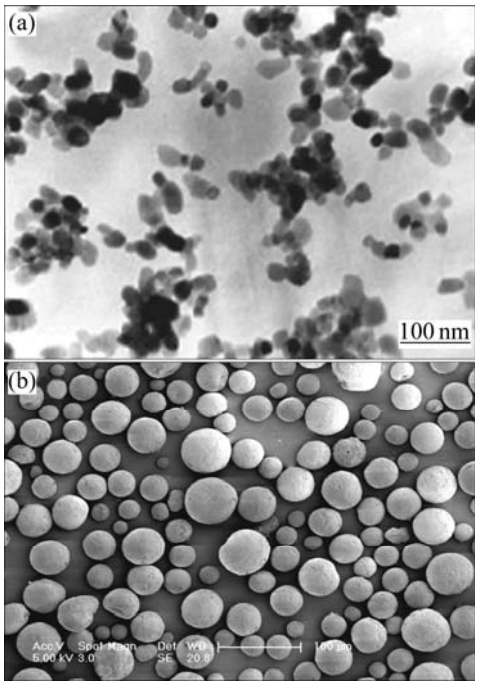

Fig.1 TEM micrograph of nanostructured YPSZ particles (a) and SEM micrograph of agglomerated YPSZ powder (b)

spraying, because an individual nanoscale particle with low mass has not enough inertia required to cross the streamlines in the spray jet. The spray-dried zirconia powders are spherical with size in a range of 20−70 μm, as seen in Fig.1(b).

Fig.2 presents the top surface morphology of the as-sprayed nanostructured coating. It can be seen that the surface is mainly formed by the melted powder in Fig.2(a). The vertical microcrack networks are observed in the melted part. The microcracks may originate due to the release of the residual stresses as molten splats solidify and cool down rapidly. The microcracks are fine and evenly distributed in the coating. It relates to increase of the toughness of the nanostructured zirconia coating. Fig.2(b) shows partially melted powder on the surface. The outer parts of the powder are melted, and many irregular shaped granules are formed and connected with each other, surrounded with many micropores. The underlying parts of the powder still retain the nanostructure of the powder.

The SEM images of fractured cross-section of the as-sprayed nanostructured coating are shown in Fig.3. It can be clearly observed in Fig.3(a) that the coating is porous and loose. Moreover, different microstructures coexist. Laminar layers with columnar grains are surrounded with unmelted parts of the nanostructured powder and some large equiaxed grains. The preserved nanostructure is in the form of agglomerates because of the poor flattening ability of the unmelted core of powder. Fig.3(b) shows the equiaxed grains with an average diameter of about 2 μm in the coating. Fig.3(c) presents the nanosized columnar grains highly bounded among each other with an average diameter of about 130 nm, similar to those of conventional coarse-grained counterparts, evolved from the fully molten and flattened powder[6−8]. Fig.3(d) shows that the initial nanostructure of powder is remained in the coating. The preexisting nanostructure and the equiaxed grains in the

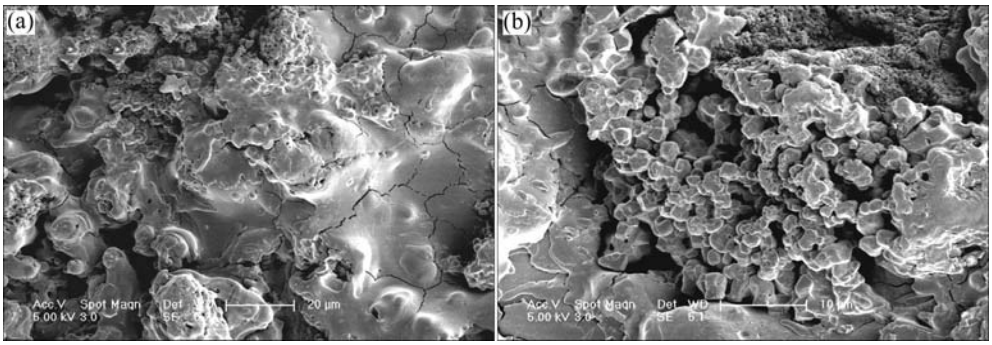

Fig.2 Top surface SEM morphologies of as-sprayed nanostructured coating

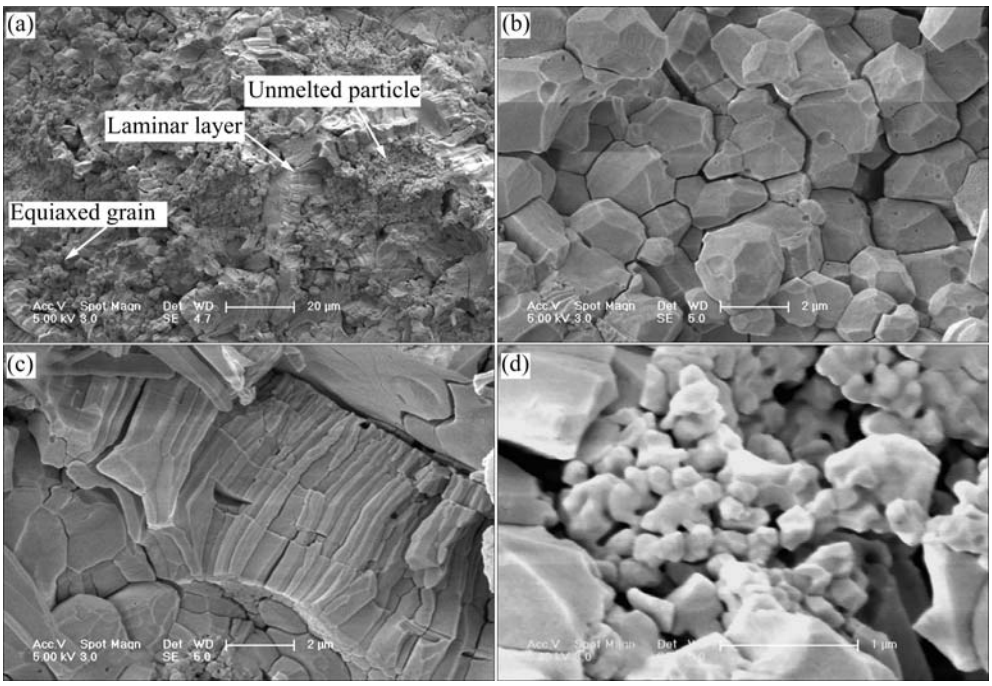

Fig.3 Fractured cross-section SEM images of nanostrucutured coating

nanostructured coating are unique, compared with the conventional counterparts. In brief, the microstructure of plasma sprayed zirconia coating from reconstituted nanostructured powder exhibits a tri-modal distribution.

As mentioned in section 2.1, in order to preserve a part of the powder's nanostructure and achieve the necessary physical condition for cohesion and adhesion, the spraying parameters have been optimized to partially melt the powder particles during plasma spraying. On the other hand, the temperature in plasma flow decreases rapidly from the core to the periphery, and the particle sizes of powder are wildly distributed. Consequently, the temperature for each particle is different during plasma spraying, which leads to the particles in plasma flow presenting different melting states, which is schematically illustrated in Fig.4. In state (a), the coarse particle at low temperatures tends to partially melt with an unmelted core due to its large mass and volume. The moderate powder, whose temperature may be approximately at the melting point during spraying, is partially melted with some unmelted solid particles or a thin unmelted core. The subsequent impacting of powder on the substrate makes the unmelted core or some big unmelted particles break into pieces and homogenously disperse in the flattened melt, as presented in state (b). The small powder at relatively high temperatures is fully melted in state (c).

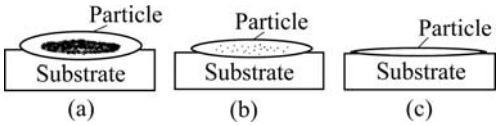

Fig.4 Schematic illustration of particle melting states during plasma spraying (Black dots stand for unmelted part)

As a result, the unmelted core of powder in state (a) will keep the powder's nanostructure intact and be mixed with the melted portion in the coating. In state (b), the small solid particles homogenously dispersed inside the molten droplets serve as the nuclei in crystallization, increasing the nucleation rates. Moreover, high cooling rates give rise to high nucleation rates. Thus, the equiaxed grains are formed. In state (c), the nanostructured powder is fully melted during spraying, and rapid heterogeneous nucleation occurs at the cooler boundaries of the flattened droplets at large undercooling. Meanwhile, an increase in temperature of the droplet, produced by the release of the heat of fusion during rapid crystal growth, will tend to suppress further nucleation because of the large temperature dependence of nucleation rate, so crystals grow from the interface into the droplet (i.e. in the opposite direction to the heat flow), forming a columnar grain structure. Such processes destroy the original nanostructured feature of the powder.

3.2 Phase analysis via X-ray diffraction

Fig.5 shows the XRD patterns of the YPSZ powder and the as-sprayed coating. The typical (111) and $(11\bar{1})$ peak can be observed in the powder pattern, which indicates that the reconstituted nanostructured powder exhibits the presence of not only the tetragonal and the cubic but also the monoclinic phases. The volume fraction of the monoclinic phase can be estimated by the following formula[14,18−19]:

$$m\% = \frac{m(11\bar{1}) + m(111)}{t(111) + m(11\bar{1}) + m(111)} \times 100\% \quad (3)$$

where the terms $m(111)$, $t(111)$ and $m(11\bar{1})$, represent the intensities of corresponding diffraction peaks in the XRD pattern, respectively. The volume fraction of the monoclinic phase in the feedstock according to the XRD pattern is approximately 28.9%. However, there is no existence of the monoclinic zirconia in the as-sprayed coating from the XRD pattern. The result shows that the nanostructured as-sprayed coating is wholly composed of the tetragonal phase. The comparison between the as-sprayed coating and the powder releases that the

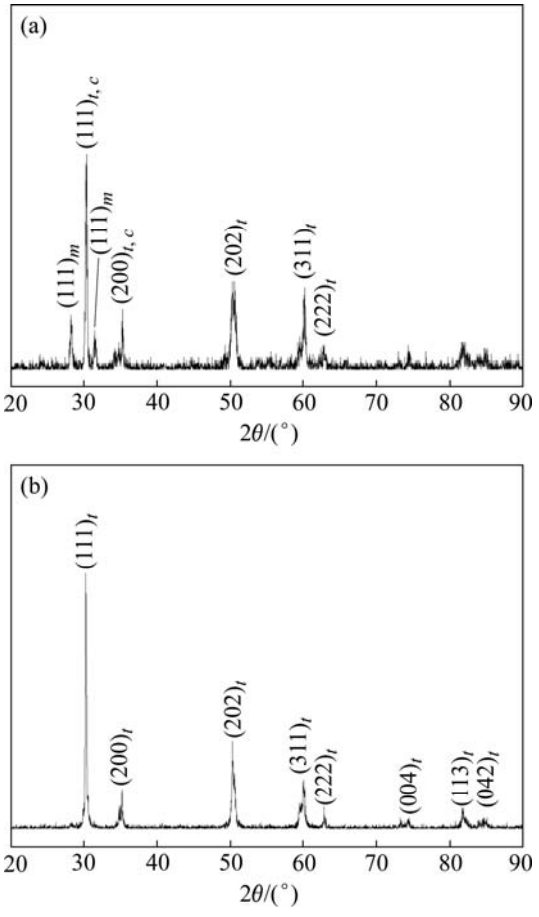

Fig.5 XRD patterns of reconstituted nanostructured powder (a)

and as-sprayed nanostructured coating (b)

remarkable phase changes have taken place during the plasma spraying process. The monoclinic phase disappears after plasma spraying, as can be explained that the rapid cooling rate, which is nearly the order of 10^6−10^7 K/s in the thermal sprayed particles[17,20], prevents the transformation of zirconia from the tetragonal to the monoclinic and makes the metastable tetragonal zirconia from the cubic via non-diffusive phase transformation. The penetration distance of the X-ray beam into the sample can reach several micrometers depending on the sample characteristics [2,17]. Therefore, a thin layer on the top surface of the ultrasonically cleaned as-sprayed coating only consists of the non-transformable tetragonal phase which is typical of plasma sprayed zirconia due to the quenching of the droplets after impacting at the substrate from high temperatures. This phenomenon was also observed by CHEN and DING[14], LIMA et al[17] and LIANG et al[19].

The (222) peak in the XRD pattern of the as-sprayed nanostructured coating was used for the mean grain size determination according to Ref.[17]. The mean grain size computed by Scherrer equation is approximately 42 nm. The grain size of the coating increases obviously after spraying because of the melting of the nanostructure powder, nucleation and growth up of grain. The grain size difference for the nanostructured powder and the coating is above 28%. The Scherrer equation is deduced under the assumption that only a small grain size is responsible for peak broadening[16]. Strain effects, which may influence the peak broadening, are not taken into account. In the thermal spray, the occurrence of the residual stress effects is evident[6−8]. So the use of Scherrer equation to measure the mean grain size of the coating may be biased by stress effects.

4 Conclusions

1) The microstructure of as-sprayed zirconia coating from the reconstituted nanostructured powder exhibits a unique tri-modal distribution including the initial nanostructure of the powder, equiaxed grains and columnar grains.

2) The air plasma sprayed nanostructured zirconia coatings consist of only the non-transformable tetragonal phase, whereas the reconstituted nanostructured powder shows the presence of the monoclinic, the tetragonal and the cubic phases. The mean grain size estimated by the XRD technique for the as-sprayed coating is about 42 nm.

Acknowledgements

The authors are grateful to the Instrumental Analysis Center, Shanghai Jiao Tong University for the samples examination.

References

[1] TJONG S C, CHEN H. Nanocrystalline materials and coatings [J]. Mater Sci Eng R, 2004, R45: 1−88.
[2] HE J H, SCHOENUNG J M. Nanostructured coatings [J]. Mater Sci Eng A, 2002, A336: 274−319.
[3] HE J, ICE M, LAVERNIA E J. Synthesis of nanostructured Cr3C2-25 (Ni20Cr) coatings [J]. Metallurgical and Materials Transaction, 2000, A31: 555−564.
[4] GELL M, JORDAN E H, SOHN Y H. Development and implementation of plasma sprayed nanostructured ceramic coatings [J]. Surface and Coatings Technology, 2001, 146/147: 48−54.
[5] JORDAN E H, DELL M, SOHN Y H. Fabrication and evaluation of plasma sprayed nanostructured alumina-titania coatings with superior properties [J]. Mater Sci Eng A, 2001, A301: 80−89.
[6] MILLER R A. Thermal barrier coatings for aircraft engines: History and directions [J]. J Thermal Spray Technology, 1997, 6(1): 35−42.
[7] PADTURE N T, GELL M, JORDAN E H. Thermal barrier coatings for gas-turbine engine application [J]. Science, 2002, 296: 280−284.
[8] GOWARD G W. Progress in coating for gas turbine airfoils [J]. Surface and Coatings Technology, 1998, 108/109: 73−79.
[9] CHEN H, ZHANG Y, DING C. Tribological properties of nanostructured zirconia coatings deposited by plasma spraying [J]. Wear, 2002, 253: 885−893.
[10] GELL M. Potential for nanostructured materials in gas turbine engines [J]. Nanostructured Materials, 1995, 6(5/8): 997−1000.
[11] SOYEZ G, EASTMAN J A, THOMPSON L J. Grain-size-dependent thermal conductivity of nanocrystalline yttria stabilized zirconia films grown by metal-organic chemical vapor deposition [J]. Appl Phys Lett, 2000, 77(8): 1155−1165.
[12] LIMA R S, KUCUK A, BERNDT C C. Evaluation of microhardness and elastic modulus of thermally sprayed nanostructured zirconia coatings [J]. Surface and Coatings Technology, 2001, 135: 166−172.
[13] ZHOU C, WANG N, WANG Z. Thermal cycling life and thermal diffusivity of a plasma sprayed nanostructured thermal barrier coatings [J]. Scripta Materialia, 2004, 51: 945−948.
[14] CHEN H, DING C X. Nanostructured zirconia coating prepared by atmospheric plasma spraying [J]. Surf Coat Technol, 2002, 150: 31−36.
[15] CHEN H, ZHOU X M, DING C X. Investigation of the thermomechanical properties of a plasma-sprayed nanostructured zirconia coating [J]. J Eur Ceram Soc, 2003, 23: 1449−1455.
[16] JIANG H G, RUHLE M, LAVERNIA E J. On the applicability of the X-ray diffraction line profile analysis in extracting grain size and microstrain in nanocrystalline materials [J]. J Material Research, 1999, 14(2): 549−559.
[17] LIMA R S, KUCUK A, BERNDT C C. Integrity of nanostructured partially stabilized zirconia after plasma spray processing [J]. Mater Sci Eng A, 2001, A313: 75−82.
[18] MASAKI T. Mechanical properties of toughened ZrO_2-Y_2O_3 ceramics [J]. Journal of the American Ceramic Society, 1986, 69(8): 638−640.
[19] LIANG B, DING C, LIAO H. Phase composition and stability of nanostructured 4.7wt% yttria-stabilized zirconia coatings deposited by atmospheric plasma spraying [J]. Surface & Coatings Technology, 2006, 200: 4549−4556.
[20] MCPHERSON R. Relationship between the mechanism of formation, microstructure and properties of plasma sprayed coatings [J]. Thin Solid Film, 1981, 83: 297−310.

(Edited by LI Xiang-qun)